A Generalized Contact Mechanics Analysis of Elastic-Plastic Spherical Indentation

L. Kogut, Post-Doctoral Fellow, Mem. ASME

K. Komvopoulos, Professor, Fellow ASME

Department of Mechanical Engineering

University of California

Berkeley, CA 94720

Abstract

A finite element analysis of frictionless indentation of an elastic-plastic half-space by a rigid sphere is presented to elucidate the deformation behavior during loading and unloading. The analysis yields dimensionless constitutive relations for the normal load, contact area, and mean contact pressure during loading for a wide range of material properties and for interference distances ranging from the inception of yielding to the initiation of fully plastic deformation. The boundaries between elastic, elastic-plastic, and fully plastic deformation regimes are determined in terms of interference distance, mean contact pressure, and reduced elastic modulus-to-yield strength ratio. Relations for the hardness and corresponding interference distance versus elastic-plastic material properties and truncated contact radius are introduced, and the shape of the plastic zone and maximum equivalent plastic strain are interpreted in the context of finite element simulation results. The unloading response of the spherical indenter is also analyzed to evaluate the validity of basic assumptions in traditional indentation approaches used to measure the hardness and reduced elastic modulus of materials. An alternative approach for determining the reduced elastic modulus, yield strength, and hardness of materials is proposed based on the obtained results.

Submitted for publication in the ASME Journal of Applied Mechanics, December 18, 2002.

1. Introduction

The elastic-plastic indentation of a homogenous half-space by a rigid sphere is a fundamental problem in contact mechanics and of particular importance in numerous materials processing and mechanics applications, such as powder compaction, contact of rough engineering surfaces, and nanoindentation hardness measurement. In powder compaction, the prediction of the global force-displacement behavior depends on knowledge of the local indentation response between particles (Vu-Quoc et al., 2000). Likewise, models for contact (Komvopoulos and Ye, 2001), adhesion (Komvopoulos and Yan, 1998), and static and dynamic friction (Chang et al., 1998; Sahoo and Roy Chowdhury, 2000) of rough surfaces are based on single-asperity constitutive relations of the contact parameters. The high level of interest in these subjects is demonstrated by the impressive number of studies published to date (Bhushan, 1996, 1998; Liu et al., 1999; Adams and Nosonovsky, 2000).

Indentation tests have been used from the beginning of the previous century to routinely measure the plastic properties of metals (Tabor, 1951). As opposed to a typical tension test, the indentation test is localized, and can be applied either to small material samples or fabricated machine parts and structural elements. In recent years, due to extensive development of depth-sensing indentation techniques, nanoindentation has been used to evaluate the mechanical properties of surface layers and thin films of different materials (Herbert et al., 2001; Huber et al., 2001; Nayebi et al., 2002). However, current nanoindentation procedures are based on simplified assumptions about the material behavior during unloading and empirical relations of the contact area (e.g., Oliver and Pharr, 1992) with little input from analytical and numerical solutions. Therefore, it is unclear what properties can be measured using instrumented indentation techniques and what is the real indentation hardness of materials.

The first indentation analysis for a purely elastic half-space is attributed to Hertz (Johnson,

1985). A solution for the spherical indentation of a rigid-perfectly plastic half-space was obtained by Ishlinsky (Johnson, 1985) using the slip-line method. Hill et al. (1989) and Biwa and Storåkers (1995) determined the similarity solution for a rigid-plastic half-space by using the deformation and flow theory, respectively. According to the similarity solution, the upper limit of the mean contact pressure, which is usually interpreted as the material hardness, is equal to three times the yield strength. However, the elasticity of real materials plays an important role in the indentation process, especially for a relatively blunt indenter such as a spherical indenter (Fischer-Cripps, 1997). Johnson (1985) analyzed the indentation response of elastic-perfectly plastic solids and reported the successive occurrence of elastic, elastic-plastic, and fully plastic deformation. Based on a simplified theoretical model and assuming fully developed plastic flow, Johnson (1985) derived a contact force-displacement relation.

Theoretical treatment of elastic-plastic indentation is cumbersome and requires simplified assumptions because the shape and size of the elastic-plastic boundary is not known a priori. This has led to the use of the finite element method in numerous studies of elastic-plastic spherical indentation (e.g., Hardy et al., 1971; Follansbee and Sinclair, 1984; Kral et al., 1993; Giannakopoulos, 2000; Kucharski and Mroz, 2001). Recently, Komvopoulos and Ye (2001) used finite element results to derive dimensionless constitutive relations for the mean contact pressure and contact area for elastic-perfectly plastic half-space indented by a rigid sphere. In the fully plastic deformation regime the mean contact pressure was found to be constant and equal to 2.9 times the yield strength, which is close to the value obtained from the similarity solution.

The use of a spherical indenter in hardness measurements is usually restricted to tests involving ductile materials. However, there is a class of nominally brittle materials that has been demonstrated to exhibit yielding in indentation tests with spherical indenters at modest loads

(Fischer-Cripps, 1997). Brittle materials, such as glass-ceramic, possess higher yield strains than ductile metals. The shape of the plastic zone in brittle materials is markedly different from that in metals. Mesarovic and Fleck (1999) have shown that the maximum value of the mean contact pressure (i.e., the material hardness) is never obtained with solids exhibiting sufficiently high yield strain. Moreover, the hardness and corresponding representative strain depend on the magnitude of the yield strain.

The aforementioned dependency of the stress field and contact parameters on the yield strain raises questions about the validity of established constitutive relations used to predict the indentation response of a wide range of materials. Thus, the main objective of the present study was to analyze the deformation behavior of different elastic-perfectly plastic materials during indentation loading and unloading. Constitutive relations for dimensionless contact parameters were derived for a half-space indented by a rigid sphere in the elastic-plastic deformation regime using finite element simulation results. The boundary between elastic-plastic and fully plastic deformation regimes, determined in terms of the mean contact pressure and corresponding interference distance, provides useful guideline for the measurement of the real material hardness in indentation experiments. In order to examine the validity of common approaches in indentation testing, finite element results for the unloading behavior are presented in terms of material properties. Simulation results are used to obtain an alternative approach for measuring the reduced elastic modulus, yield strength, and material hardness.

2. Theoretical Background

Figure 1 shows a rigid sphere of radius R indenting an elastic-perfectly plastic half-space. The interference distance, d, and contact radius, r, correspond to a normal load, P. The displacement

of the contact edge measured from the original surface, h, is assumed to be positive if the material deforms as shown in the figure. The mean contact pressure, p_m, is defined as

$$p_m = \frac{P}{a}, \tag{1}$$

where a is the contact area. For dimensionless analysis, the interference, contact area, and mean contact pressure are normalized by the radius of the truncated contact area, r', truncated contact area, a', and material yield strength, Y, respectively. The truncated contact area is given by

$$a' = \pi r'^2 = \pi d(2R - d). \tag{2}$$

For small interference, i.e., $d / r' < 1.78/(E/Y)$, the indentation response is elastic, and according to Hertz theory,

$$\frac{p_m}{Y} = \frac{4\sqrt{2}}{3\pi}\left(\frac{Ed}{Yr'}\right) \text{ and } \frac{a'}{a} = 2, \tag{3}$$

where E is the reduced elastic modulus, given by $E = \left[\left(1-n_1^2\right)/E_1 + \left(1-n_2^2\right)/E_2\right]^{-1}$, in which E_1, E_2 and n_1, n_2 are the elastic moduli and Poisson's ratios of the two materials, respectively. In the case of a rigid indenter, $E_2 \to \infty$. The dimensionless material parameter E/Y in Eq. (3) is related to the yield strain of the half-space, Y/E_1. However, E_1 is replaced by E in order to combine the two elastic properties (i.e., E_1 and n_1) into one elastic parameter, as suggested by Hertz. Experiments (Johnson, 1970) and numerical results (Johnson, 1985) suggest that the reduced elastic modulus, E, adequately describes the elastic contribution to deformation in the elastic-plastic deformation regime. Mesarovic and Fleck (1999) observed that the reduced elastic modulus is appropriable for describing the contact area in the elastic-plastic deformation regime.

When the dimensionless interference reaches a critical value, $d / r' = 1.78/(E/Y)$, yielding commences in the half-space below the center of the contact region and the corresponding mean

contact pressure is $p_m/Y = 1.07$ (Komvopoulos and Ye, 2001). With increasing interference, the elastic-plastic indentation response is gradually dominated by plastic flow. The inception of fully plastic deformation is encountered when the mean contact pressure first reaches its upper limit, i.e., the material hardness, H. Johnson (1970) argued that deformation in elastic-plastic indentation depends on the ratio of the representative strain below the indenter, r/R, to the yield strain of the half-space, Y/E. Similarly to the elastic Hertz solution, two elastic properties are combined into one elastic parameter, E, and the indentation is characterized by a single dimensionless parameter, Er/YR. However, Mesarovic and Fleck (1999) reported that for a given value of Er/YR, different values of E/Y yield different results for the contact parameters. Moreover, the dimensionless parameter Er/YR, suggested by Johnson (1970) to describe the indentation behavior, contains the unknown radius of the contact area, r. Mesarovic and Fleck (1999) have also shown that the boundary between the elastic-plastic and the fully plastic deformation regimes cannot be defined by a single dimensionless parameter, as in previous studies (Johnson, 1985; Komvopoulos and Ye, 2001).

The most frequently measured mechanical properties using load and interference sensing indentation techniques are the hardness and reduced elastic modulus. In a commonly used method (Oliver and Pharr, 1992), indentation load versus displacement data are obtained for one complete load/unload cycle of arbitrary maximum load, P_{max}. The material hardness is then determined as $H=P_{max}/a$, where a is the contact area corresponding to P_{max}. Since a cannot be measured during loading, methods for estimating the contact area from the indenter shape function have been proposed (e.g., Oliver and Pharr, 1992). In the case of a relatively small interference, a spherical indenter can be approximated as a paraboloid of revolution and, according to the elastic analysis of Sneddon (1965) and Oliver and Pharr (1992), the contact depth, h_c (Fig. 1), is given by

$$h_c = d - 0.75\frac{P_{\max}}{S},$$

where S is the experimentally measured stiffness at the inception of unloading. From geometric considerations, the contact area, a_s (hereafter referred to as the shape function of the indenter), is

$$a_s = ph_c(2R - h_c). \tag{4}$$

Alternatively, the contact area can be approximated by the residual impression area, a_i, assuming negligible surface recovery (Thurn et al., 2002).

The analysis of the unloading data is based on the assumption that unloading is fully elastic and during the initial withdrawal of the indenter, the contact area remains constant. For this case, Hertz theory (Johnson, 1985) can be used to determine the reduced elastic modulus

$$E = \frac{\sqrt{p}}{2}\frac{S}{\sqrt{a}}, \tag{5}$$

where a in Eq. (5) is the contact area corresponding to the arbitrary maximum indentation load, P_{max}.

3. Finite Element Modeling

A finite element model of a rigid sphere indenting a homogeneous half-space was used to determine the mean contact pressure and contact area as functions of interference distance. The multi-purpose code ABAQUS was used to perform the finite element simulations. The following assumptions were adopted in the finite element analysis: (a) perfectly smooth surfaces, (b) frictionless contact, (c) homogenous, isotropic, elastic-perfectly plastic half-space following the J_2 flow theory, (d) sufficiently small yield strain (i.e., less than 10%) in order for yielding to commence without the occurrence of finite deformation (Mesarovic and Fleck, 1999), and (e) negligible adhesion forces at the contact region. An elastic-plastic constitutive model that satisfies the J_2 plastic flow theory was used in the finite element simulations, based on the assumption that the deformation

gradient can be decomposed into elastic and plastic parts using a multiplicative decomposition. According to the von Mises yield criterion, yielding occurs when

$$f = J_2 - k^2 = 0,$$

where k is a material constant equal to $Y/\sqrt{3}$, and J_2 is the second invariant of the deviatoric stress tensor, S_{ij}, given by

$$J_2 = \frac{1}{2} S_{ij} S_{ij},$$

where $S_{ij} = s_{ij} - \frac{1}{3} d_{ij} s_{kk}$, in which, d_{ij} is the Kronecker delta, and s_{kk} is the sum of the three normal stress components. In terms of the uniaxial yield strength, the yield criterion reduces to

$$s_{eq} = \left[\frac{3}{2} S_{ij} S_{ij} \right]^{1/2} = Y,$$

where s_{eq} is the von Mises equivalent stress. The material model used to describe plastic deformation was based on the flow rule

$$de_{ij}^{p} = dl\, S_{ij},$$

where de_{ij}^{p} are components of the plastic strain increment, and dl is a function of the flow stress and the plastic strain rate. The equivalent plastic strain, e_{eq}, is defined as

$$e_{eq} = \int_{\Omega} \left[\frac{2}{3} de_{ij}^{p} de_{ij}^{p} \right]^{1/2}, \qquad (6)$$

where the integration in Eq. (6) is carried out over the strain path, Ω. The usual assumption of negligible plastic volume change was maintained. The J_2 flow theory applies only to yielding material for which $s_{eq} = Y$. When $s_{eq} < Y$, the usual elastic constitutive equations are used.

The rigid contact surface option was used to simulate the rigid indenter. The half-space was

modeled by 12,063 axisymmetric, eight-node, quadratic, isoparametric elements consisting of 34,337 nodes (Fig. 2). Contact between the indenter and the half-space surface was detected by special contact elements. The nodes on boundaries y = 0 and x = 0 were constraint against displacement in the x-and y-direction, respectively. The resolution of the finite element mesh can be evaluated in terms of the half distance between two adjacent nodes divided by the determined contact radius. The resolution obtained with the mesh shown in Fig. 2 was better than 2.5% for all material properties and load cases simulated in the present study. To account for nonlinearities due to the material nonlinear behavior (plasticity), geometric nonlinearities (i.e., large displacements), and surface contact, an updated Lagrangian formulation was used in the finite element analysis. The typical computation time for a simulation on a Pentium III 550 computer was approximately 40,000 CPU seconds.

In order to generalize the numerical solutions and eliminate the dependency of the results on input parameters, the global contact parameters and material properties are presented in dimensionless form, i.e., p_m/Y, a'/a, d/r', and E/Y. The validity of this normalization was evaluated comparing finite element solutions obtained for different values of R, d, E, and Y, yielding identical values of d/r' and E/Y. The results for p_m/Y and a'/a versus dimensionless interference, d/r', for a given E/Y value were always the same regardless of the selection of the indenter radius, interference distance, and elastic-plastic material properties.

Figure 3 shows a comparison between results for the dimensionless mean contact pressure, p_m/Y, obtained from the present finite element model and the classical Hertz theory (Eq. (3)) for E/Y = 11 in the elastic deformation regime (i.e., $d/r' < 1.78/(E/Y)$). The results are in good agreement, with the maximum difference being less than 6.5%. The inception of yielding occurs when $d/r' = 1.78/(E/Y) = 0.162$, and the yield point is located below the center of the contact area,

as predicted by the Hertz theory (Johnson, 1985). Similar small differences between theoretical and finite element results were obtained for the dimensionless contact area, a'/a. The largest difference of 6.5% was found to be due to an overestimation of the analytical contact radius by 3.2%. It should be mentioned that for this specific material (E/Y = 11) the radius of the contact area at the inception of yielding is equal to 0.22R, which may violate the assumption in the Hertz analysis that the contact area is much less than the radius of the indenter. However, even for such relatively large contact radius of r/R = 0.22, the difference between theoretical and numerical results is less than 3% and the Hertz solution is still valid. The favorable comparison of the numerical and theoretical results illustrates the suitability of the finite element model and correctness of the assumed boundary conditions.

4. Results and Discussion

In this section, results corresponding to the deformation behavior during indentation loading and unloading are presented separately in order to facilitate the analysis of the material response. Subsequently, an analytical treatment based on the obtained results is introduced to provide guideline for the accurate determination of the mechanical properties from the material indentation response.

4.1 Loading Behavior

The dependence of the mean contact pressure, p_m/Y, on interference, d/r', is shown in Fig. 4 for different material properties in the range of $11 \le E/Y \le 450$. The lower limit ($E/Y = 11$) was chosen in order to satisfy the assumption of sufficiently small yield strain (section 3), while the upper limit (E/Y = 450) was selected due to the close agreement of the results with those of the similarity solution. The maximum dimensionless contact pressure for E/Y = 450 is p_m/Y = 2.85,

which is quite close to that obtained from the similarity solution (Hill et al., 1989; Biwa and Storåkers, 1995), $p_m/Y = 3$. For materials with $E/Y > 450$, well into the elastic-plastic deformation regime, the elastic strains can be neglected in favor of the plastic strains and the materials may be treated as rigid-perfectly plastic, for which the similarity solution is a good approximation.

Figure 4 shows that yielding commences when $p_m/Y = 1.07$, i.e., $d/r' = 1.78/(E/Y)$, as predicted by the Hertz theory. This is the lower bound of the elastic-plastic deformation regime. The upper bound of the elastic-plastic deformation regime is defined by the inception of fully plastic deformation, determined by the interference distance at which the mean contact pressure reaches its maximum value for the first time (i.e., the material hardness). By curve fitting the numerical results of the maximum contact pressure, the hardness can be expressed in terms of the reduced elastic modulus and yield strength as,

$$\frac{H}{Y} = 0.201 \ln\left(\frac{E}{Y}\right) + 1.685 \ , \tag{7}$$

while the corresponding interference at the inception of fully plastic deformation is given by

$$\frac{d}{r'} = \frac{1}{1 + 0.037(E/Y)} \ . \tag{8}$$

Figure 5 shows a comparison between finite element results (both individual data and the curve corresponding to Eq. (7) are plotted in the figure) and results from a previous study (Ye and Komvopoulos, 2003) for the dimensionless hardness, H/Y, versus material properties, E/Y. The results are in fair agreement, and the trend for the hardness to increase with the reduced elastic modulus-to-yield strength ratio is similar to that observed by Marsh (1964) from Vickers indentation tests with various materials. In general, the material hardness is a system property that depends on the indenter geometry, elastic properties of contacting materials (through the reduced elastic modulus), and yield strength of the indented material. For the limiting case of a spherical rigid

indenter and a rigid-perfectly plastic half-space, the hardness is given by the similarity solution and is equal to 3Y, i.e., independent of the elastic material properties. However, the hardness of materials with E/Y < 270 is much less than 3Y. The deviation from the similarity solution increases as E/Y decreases, demonstrating a significant effect of elastic deformation on the indentation behavior of these materials. For very small values of E/Y, the indentation response is dominated by the elastic response and the hardness approaches the maximum contact pressure predicted by the Hertz solution (p_m/Y = 1.07). The results obtained from Eq. (7) are more accurate than those of a previous finite element analysis (Ye and Komvopoulos, 2003) due to the finer mesh used in the present study and the larger number of numerical data in the vicinity of the hardness point (Fig. 4) that improved the accuracy in the determination of the material hardness. The maximum discrepancy between the hardness predicted in this study and the previous analysis (Ye and Komvopoulos, 2003) is 18% and occurs for E/Y = 11.

Figure 6 shows the boundaries of the elastic-plastic deformation regime with the fully plastic (Eq. (8)) and elastic ($d/r' = 1.78/(E/Y)$) deformation regimes. The dimensionless interference, d/r', at the inception of fully plastic deformation increases with decreasing E/Y, i.e., larger interference is required to reach fully plastic deformation in the case of materials exhibiting a dominant elastic behavior. The range of dimensionless interference corresponding to the elastic and elastic-plastic deformation regimes decreases with increasing E/Y. This is because high values of E/Y represent low yield strains, and, thus, the inception of yielding and fully plastic deformation occurs at relatively smaller interference distances.

Figure 7 shows the dimensionless contact area, a'/a, as a function of dimensionless interference, d/r', in the elastic-plastic deformation regime. The dimensionless contact area approaches values close to 1 with the increase of the interference, especially for higher values of

E/Y, where the material behavior can be approximated as rigid-perfectly plastic and the contact area is equal to the truncated area. As the ratio E/Y decreases, the contribution of the elastic response to the deformation behavior becomes dominant and the ratio a'/a approaches values close to 2, corresponding to the elastic Hertz solution. The results shown in Fig. 7 indicate that the assumption that in the fully plastic deformation regime the edge of the contact area does not exhibit pile-up or sink-in (Johnson, 1985), and therefore $a'/a = 1$, is a good approximation when $E/Y \geq 270$.

The simulation results shown in Figs. 4 and 7 were used to derive relations for the dimensionless mean contact pressure and contact area in terms of dimensionless interference and material properties. From curve fitting, the following constitutive relations were obtained for the elastic-plastic deformation regime, in which $1.78/(E/Y) \leq d/r' \leq [1+0.037(E/Y)]^{-1}$,

$$\frac{p_m}{Y} = 0.839 + \ln\left[\left(\frac{E}{Y}\right)^{0.656}\left(\frac{d}{r'}\right)^{0.651}\right], \tag{9}$$

and

$$\frac{a'}{a} = 2.193 - \ln\left[\left(\frac{E}{Y}\right)^{0.394}\left(\frac{d}{r'}\right)^{0.419}\right]. \tag{10}$$

The maximum differences between the results obtained from Eqs. (9) and (10) and the numerical results shown in Figs. 4 and 7 were found when E/Y = 11 (with average error equal to 5.3% and 6.4%, respectively). The constitutive relation for the contact load, P, can be derived by multiplying the mean contact pressure (Eq. (9)) by the contact area (Eq. (10)). Hence, the dimensionless contact load, $P/(a'Y)$, can be expressed as

$$\frac{P}{a'Y} = \frac{0.839 + \ln\left[\left(\frac{E}{Y}\right)^{0.656}\left(\frac{d}{r'}\right)^{0.651}\right]}{2.193 - \ln\left[\left(\frac{E}{Y}\right)^{0.394}\left(\frac{d}{r'}\right)^{0.419}\right]}. \tag{11}$$

Results for the mean contact pressure and contact area obtained from Eqs. (9) and (10), respectively, were found to be in good agreement with finite elements results reported by Komvopoulos and Ye (2001) for high E/Y values. However, large differences (up to 26%) were obtained with low E/Y values. In particular, the boundary between the elastic-plastic and fully plastic deformation regimes reported in the previous study (Komvopoulos and Ye, 2001), $d/r' = 21/(E/Y)$, differs significantly from that found in this work (Eq. (8)). Presenting the results for the boundary between the elastic-plastic and fully plastic deformation regimes in terms of a single dimensionless parameter yields $7.8 \le Ed/Yr' \le 25.4$ for materials with $11 \le E/Y \le 450$. This shows that a single dimensionless parameter, Ed/Yr', is not adequate to uniquely determine the evolution of deformation in the elastic-plastic deformation regime. Therefore, it is essential to decompose the previous dimensionless parameter into two dimensionless parameters, d/r' and E/Y, in order to accurately describe the elastic-plastic response over a wide range of material properties. The large differences between the results of the present model and those of Komvopoulos and Ye (2001) may be due to the high magnitude of E/Y used in the earlier study, as evident from the high value of the mean contact pressure in the fully plastic deformation regime, i.e., $p_m/Y = 2.9$. Therefore, the constitutive relation for elastic-plastic deformation of Komvopoulos and Ye (2001) may be considered to be a limiting case of the present general solution and adequate for materials with $E/Y \ge 379$.

Similar to the global contact parameters, a strong effect of the material properties was found for the subsurface parameters, such as shape of plastic zone and magnitude and location of maximum equivalent plastic strain. Figures 8(a) and 8(b) show plastic regions below the spherical indenter at the inception of fully plastic deformation for E/Y = 11 and 450, respectively. For E/Y = 11, the plastic region is confined below the contact area, whereas for E/Y = 450, the plastic

region extends beyond the contact area to the surface of the half-space. It was found that the plastic region gradually grows outside the contact edge with the increase of E/Y. This transition is in good agreement with experimental results for mild steel and glass-ceramic specimens presented by Fischer-Cripps (1997). From Figs. 8(a) and 8(b) it can be observed that in the elastic-plastic deformation regime the contact edge either moves downward ($a'/a > 1$) or remains at the level of the original surface ($a'/a \approx 1$) when E/Y assumes relatively low or high values, respectively.

Figure 9 shows the variation of the maximum equivalent plastic strain, $e_{eq}^{\max}$ (Eq. (6)), with material properties, E/Y, at the inception of fully plastic deformation. Results for the representative strain, Er/YR (Johnson, 1970), are also plotted for comparison. The increase of $e_{eq}^{\max}$ with E/Y confirms the dominance of plastic flow in materials exhibiting low yield strain. A plastic strain plateau $e_{eq}^{\max}/(Y/E) \approx 40$ is reached when E/Y > 270. The representative strain has the same trend as $e_{eq}^{\max}$, and the value used by Johnson (1985) to determine the inception of fully plastic deformation, $Er/YR \approx 40$, is a good approximation only for materials with $E/Y \approx 160$, while it largely overestimates the representative strain at the inception of fully plastic deformation when E/Y < 160.

Figure 10 shows the dependence of the radial distance, x/a, of the material point with the maximum equivalent plastic strain on material properties at the inception of fully plastic deformation. For all materials, the initial location of $e_{eq}^{\max}$ at the inception of yielding is below the center of the contact area (x/r = 0), as predicted by the Hertz theory, and shifts gradually toward the location shown in Fig. 10 with the increase of the interference. When the indentation behavior is dominated by the elastic response (e.g., E/Y = 11), the location of $e_{eq}^{\max}$ is approximately below the center of the contact area, similar to the location of the equivalent elastic strain in the case of purely

elastic deformation (Hertz solution). However, the radial distance of $e_{eq}^{\max}$ increases with E/Y, reaching the edge of the contact area $(x/r \approx 1)$ when E/Y > 160.

Although the present work is mainly focused in the elastic-plastic indentation response, an interesting phenomenon worthy of discussion was observed in the fully plastic deformation regime. As shown in Fig. 4, for intermediate values of E/Y, the mean contact pressure decreases immediately after reaching a peak value, whereas for both low and high values of E/Y, it remains almost constant after reaching a maximum, at least for the examined interference range. The decrease of p_m after reaching a peak value can be explained by considering the increase of the contact area due to the occurrence of pile-up at the contact edge. As shown in Fig. 8(a), plastic deformation in materials with low E/Y is restricted below the contact area and the free surface moves downward during indentation loading. However, materials with high E/Y are relatively more rigid and the movement of the free surface is negligible (Fig. 8(b)).

4.2 Unloading Behavior

The unloading response of the indented half-space was analyzed from a maximum interference distance, d_i, corresponding to the inception of fully plastic deformation of each material case (unless otherwise stated) to an interference distance, d_f, corresponding to zero normal load. The surface recovery, global contact parameters, and equivalent plastic strain were tracked during unloading in order to evaluate the effect of material properties on the deformation behavior during the retraction of the indenter. For most material cases, the residual vertical displacement of the center point of the impression after complete unloading, d_r, was found to be equal to d_f. During the initial stage of unloading, the surface of the deformed medium begins to separate from the indenter at the edge of the contact area. With continuing unloading, the separation point moves toward the

center of the contact area and the last point to separate from the indenter is the center point of the residual impression; thus, $d_r = d_f$. While surface separation during unloading for E/Y = 11 commenced at the contact edge, as with the other material cases, it was found that $d_f < d_r$. This is because the maximum equivalent plastic strain occurs approximately below the center of the impression, restricting the elastic recovery of this material point. During unloading, the elastic recovery at the center point is exhausted, while other surface points are still in contact with the indenter. A zero normal load is obtained at interference distance $d_f < d_r$ when all the surface nodal points of the half-space have separated from the spherical indenter.

The elastic recovery of the indented material can be characterized by the change of the displacement at the center of the contact area, E_{Rd}, defined as

$$E_{Rd} = \frac{d_i - d_r}{d_i}. \tag{12}$$

Another parameter to quantify the elastic recovery is the ratio of the released energy during unloading and the total input energy during loading, E_{RE}, defined as

$$E_{RE} = \frac{\int_{d_f}^{d_i} P(d)dd}{\int_{0}^{d_i} P(d)dd}. \tag{13}$$

While the elastic recovery can be easily determined from Eq. (12), this is based solely on the displacement of the center point of the residual impression that may not be representative of the recovery of the entire surface. However, estimation of the elastic recovery using Eq. (13) is representative of the global elastic recovery, although calculation is somewhat more complex. Figure 11 shows a comparison between numerical results obtained from Eqs. (12) and (13) for the range of material properties examined in this study. The agreement between the results of the two methods is

fairly good. As expected, the elastic recovery decreases with increasing E/Y because less elastic strain energy is stored in materials exhibiting low yield strain. From curve fitting of the numerical results shown in Fig. 11, the material elastic recovery can be obtained from the following semi-empirical relations

$$E_{Rd} = 0.591\left(\frac{E}{Y}\right)^{-0.156} \text{ and } E_{RE} = 0.616\left(\frac{E}{Y}\right)^{-0.176}.$$

Finite element results (not shown here for brevity) confirmed that, for all material cases, the elastic recovery increased when unloading was initiated from a smaller interference distance, reaching a value of 1 when unloading commenced from interferences in the elastic deformation regime. An opposite trend was found when the unloading process was initiated from interference in the fully plastic deformation regime.

A few additional observations related to the profound elastic recovery of materials exhibiting low E/Y values are worthy of discussion. First, $e_{eq}^{\max}$ increased during unloading of materials with low E/Y, indicating that unloading was not purely elastic. The increase of the plastic strain was found to occur during the last stage of unloading only for E/Y = 11 and 22. For these material cases, reloading (after complete unloading) up to the inception of fully plastic deformation produced $e_{eq}^{\max}$ higher than that obtained after the first full unloading. However, despite the occurrence of limited plasticity during reloading, the global contact parameters were similar to those obtained during unloading. Second, it was found that during the initial stage of unloading, the contact area is greater than that during loading at the same interference, despite the lower contact load during unloading at a given interference. This phenomenon could be significant in contact problems dealing with electrical and thermal conductivity, where establishing a large contact area under a given contact load is of importance. The present results suggest that this can be accomplished by an overloading of

the contacting surfaces, followed by a partial unloading to the desired load. Growth of the contact area during the initial stage of unloading was found to be negligible for materials with $E/Y \geq 270$. Third, as shown in Fig. 8(a), despite the downward displacement of the free surface during indentation loading of materials with low E/Y values, an upward movement of the surface (pile-up) was obtained upon unloading. However, for materials possessing high E/Y, this phenomenon is negligible (Fig. 8(b)). This can explain the increase of the contact area during the initial stage of unloading of indented materials with low E/Y, as discussed previously. The aforementioned behaviors and trends during unloading vanish when d_i approaches values in the elastic deformation regime, even in the case of E/Y = 11.

4.3 Determination of Mechanical Properties from the Material Indentation Response

The present finite element analysis can be extended to examine the conditions under which the assumptions used in traditional indentation approaches for measuring the reduced elastic modulus and hardness are valid. The evaluation comprises indentation loading up to the inception of fully plastic deformation, where the material hardness should be measured, followed by full unloading. As discussed in section 2, a major assumption in indentation hardness measurement is that the impression area after unloading is similar to the contact area at maximum indentation load, i.e., the surface recovery after full unloading is negligible. However, as shown in Fig. 8(a), the elastic recovery may be significant, particularly for materials exhibiting low E/Y values. The area of the residual impression, a_i, is calculated as the area of a circle with radius equal to the distance between the center point of the impression to the highest surface point after complete unloading. Figure 12 shows the error in contact area, e_a, (determined from the residual impression area, a_i, and the indenter shape function, a_s, both corresponding to the inception of fully plastic deformation)

versus material properties, E/Y. The error is greater for small values of E/Y because these materials exhibit significant sink-in and pile-up behaviors during loading and unloading, respectively (Fig. 8(a)), thus producing a larger difference between the contact areas obtained under maximum indentation load, a, and after full unloading, a_i. For E/Y > 50, the relative error is less than 5.7%, and therefore the impression area, a_i, is a good approximation of the contact area in the case of these materials.

Another approach is to use the contact area determined from the indenter shape function, a_s (Eq. (4)). As discussed in section 2, Eq. (4) is based on the assumption of purely elastic deformation and small surface interference because it includes h_c, which is obtained from a linear elastic analysis. However, the interference distance and plastic region at the inception of fully plastic deformation may be large, depending on the magnitude of E/Y (Figs. 6 and 8(b)). Figure 12 shows that the error between a_s and a is less than 5.7% when E/Y < 50 and, therefore, the approximation of the spherical indenter by a paraboloid of revolution is acceptable, even for a large interference distance. However, for E/Y > 50, the accuracy of Eq. (4) decreases, probably due to extension of the plastic region beyond the contact edge to the free surface of the half-space (e.g., Fig. 8(b)).

Figure 13 shows the error between calculated and actual reduced elastic modulus, e_E, versus material properties, E/Y. The reduced elastic modulus is calculated from Eq. (5), using the contact area at the inception of unloading, a, the area of the residual impression, a_i, and the contact area obtained from the shape function of the spherical indenter, a_s (Eq. (4)), all corresponding to the inception of fully plastic deformation. According to finite element results (not shown here), during the initial withdrawal of the indenter the contact area remains almost constant, especially for low E/Y values, due to the transition from sink-in to pile-up of the surface (Fig. 8(a)). However, this effect becomes less pronounced with increasing E/Y due to the decrease of the elastic recovery (Fig.

11) and the more rigid-like behavior inhibiting pile-up formation at the contact edge (Fig. 8(b)). Therefore, the basic assumption behind Eq. (5) is satisfied, at least for small values of E/Y, and the reduced elastic modulus can be determined with good accuracy.

When using the contact area, a, the accuracy of Eq. (5) increases with decreasing E/Y, i.e., material response is dominated by the elastic response. The accuracy for E/Y < 22, is slightly reduced, presumably due to plastic deformation during unloading, as shown by the increase of $e_{eq}^{\max}$. As explained previously, for high values of E/Y, the contact area does not remain constant during the initial stage of unloading, and, hence, the accuracy of Eq. (5) decreases. Regarding the error in Eq. (5) when using the impression area, a_i, to determine the reduced elastic modulus, the error is relatively larger than that of the other two approaches, especially for materials with low E/Y. Significantly lower error is produced with the shape function, a_s. The reduced elastic modulus can be predicted from Eqs. (4) and (5) with accuracy better than 6.3% when the unloading is initiated from a maximum load in the elastic or elastic-plastic deformation regimes. However, unloading from interference distances well within the fully plastic deformation regime increases the error for all materials in the range of $11 \le E/Y \le 450$ due to extensive plastic deformation.

As discussed earlier, applying an arbitrary maximum indentation load for measuring the material hardness may yield a mean contact pressure less than the actual hardness. This problem may be encountered in the case of light indentation loads, as in hardness measurement of very thin films, where very shallow impressions must be produced to avoid the substrate effect on the hardness measurement (Ye and Komvopoulos, 2003). However, as shown in Fig. 4, if the dimensionless interference is less than the value corresponding to the inception of fully plastic deformation (Eq. (8)), the mean contact pressure is less than the material hardness. Alternatively, applying a dimensionless interference greater than the critical value given by Eq. (8) may yield a mean contact

pressure in the fully plastic deformation regime that might be much less than the material hardness, especially for intermediate values of E/Y.

The dimensionless interference corresponding to the real material hardness is given by Eq. (8) and the corresponding indentation load can be calculated from Eq. (11). However, in order to use Eqs. (8) and (11), it is necessary to measure first the reduced elastic modulus and yield strength. As explained earlier, Eq. (5) yields fairly accurate estimates of the reduced elastic modulus over a wide range of E/Y. However, it is preferred to calculate the reduced elastic modulus from the elastic indentation response using the Hertz solution for a single load path,

$$E = \frac{3}{4}\frac{P}{R^{1/2}d^{3/2}}. \qquad (14)$$

Equation (14) may also be used to find the indenter radius if the material elastic properties are known a priori. Then, the hardness may be determined from an iterative procedure involving an initial assumption for the value of Y, calculation of the dimensionless interference, d/r', at the inception of the fully plastic deformation regime (Eq. (8)), and estimation of the corresponding dimensionless contact load, $P/a'Y$ (Eq. (11)). Next, the new value of the interference distance is measured experimentally based on the estimated contact load, and the new value of Y is calculated from Eq. (8) (or Fig. 6). This procedure can be repeated until a convergence to a specific tolerance is reached. Finally, the material hardness can be determined by substituting the obtained values of the reduced elastic modulus and yield strength in Eq. (7) or from using Fig. 5.

5. Conclusions

A finite element contact analysis of a rigid spherical indenter and an elastic-perfectly plastic half-space that is based on constitutive laws for the relevant deformation regime was performed in order to elucidate the effect of material properties on the indentation response during loading and unloading. The validity of the axisymmetric finite element model was verified by favorable

comparisons with the Hertz solution. Simple analytical expressions that extend the classical Hertz solution up to the fully plastic deformation regime were derived for a wide range of material properties. General solutions that are independent of specific material properties and radius of the spherical indenter were obtained based on a normalization scheme. In view of the presented results and discussion, the following main conclusions can be drawn.

(1) The boundaries between elastic, elastic-plastic, and fully plastic deformation regimes were determined in terms of dimensionless interference, mean contact pressure, and material properties. The boundary between elastic-plastic and fully plastic deformation regimes is of particular interest because it provides a means of extracting the material hardness. It was shown that the hardness is less than the traditionally quoted value of three times the yield strength. Equations for the hardness and corresponding dimensionless interference were obtained in terms of material properties and truncated contact radius.

(2) The shape of the plastic region and the magnitude and location of the maximum equivalent plastic strain, $e_{eq}^{\max}$, strongly depend on the reduced elastic modulus-to-yield strength ratio, E/Y. For high E/Y values, the plastic region extends beyond the contact edge to the free surface of the half-space and $e_{eq}^{\max}$ occurs at the contact edge. For small E/Y values, the plastic region is confined below the contact area and $e_{eq}^{\max}$ arises below the center of contact near the axis of symmetry. At the inception of fully plastic deformation, a constant value of $e_{eq}^{\max}$ equal to $\sim 40(Y/E)$ is reached for materials with E/Y > 270. The value of the representative strain, $Er/YR \approx 40$, suggested by Johnson (1985) for the inception of fully plastic deformation is a good approximation only for materials with $E/Y \approx 160$; however, it largely overestimates the actual value of the representative strain at the inception of fully plastic deformation when E/Y < 160.

(3) The unloading response of a spherical indenter was analyzed in order to examine the validity of basic assumptions invoked in traditional indentation approaches for measuring the hardness and reduced elastic modulus. Significant elastic recovery was found for materials possessing low E/Y. Good correlation was observed between the elastic recovery predicted based on the vertical displacement at the center of the contact area and the ratio of the elastic energy released upon unloading to the total energy stored in the material under maximum indentation load. The effect of the elastic recovery on subsurface plasticity, contact area, and transition from surface sink-in (loading) to pile-up (unloading) was explained in the context of results for different material properties.

(4) The accuracy of approximate methods for calculating the contact area and reduced elastic modulus was examined, and the conditions under which these methods yield accurate predictions were determined. The common approach used to extract the reduced elastic modulus from indentation experiments yield accurate results. However, because of inherent limitations, an alternative approach for determining the mechanical properties from indentation measurements was introduced together with an iterative procedure to obtain the yield strength and hardness in terms of the measured reduced elastic modulus.

Acknowledgements

This research was supported by the Computer Mechanics Laboratory at the University of California at Berkeley. The financial support provided to the first author (L.K.) by a Fulbright Fellowship and a New-England (Technion) award is also gratefully acknowledged.

References

Adams, G. G., and Nosonovsky, M., 2000, "Contact Modeling – Forces," Tribology International, 33, pp. 431-442.

Bhushan, B., 1996, "Contact Mechanics of Rough Surfaces in Tribology: Single Asperity Contact," ASME Journal of Applied Mechanics Reviews, 49, pp. 275-298.

Bhushan, B., 1998, "Contact Mechanics of Rough Surfaces in Tribology: Multiple Asperity Contact," Tribology Letters, 4, pp. 1-35.

Biwa, S., and Storåkers, B., 1995, "An Analysis of Fully Plastic Brinell Indentation," Journal of the Mechanics and Physics of Solids, 43, pp. 1303-1333.

Chang, W. R., Etsion, I., and Bogy, D. B., 1988, "Static Friction Coefficient Model for Metallic Rough Surfaces," ASME Journal of Tribology, 110, pp. 57-63.

Fischer-Cripps, A. C., 1997, "Elastic-Plastic Behavior in Materials Loaded with a Spherical Indenter," Journal of Materials Science, 32, pp. 727-736.

Follansbee, P. S., and Sinclair, G. B., 1984, "Quasi-Static Normal Indentation of an Elasto-Plastic Half-Space by a Rigid Sphere. Part 1: Analysis," International Journal of Solids and Structures, 20, pp. 81-91.

Giannakopoulos, A. E., 2000, "Strength Analysis of Spherical Indentation of Piezoelectric Materials," ASME Journal of Applied Mechanics, 67, pp. 409-416.

Hardy, C., Baronet, C. N., and Tordion, G. V., 1971, "The Elasto-Plastic Indentation of a Half-Space by a Rigid Sphere," International Journal for Numerical Methods in Engineering, 3, pp. 451-462.

Herbert, E. G., Pharr, G. M., Oliver, W. C., Lucas, B. N., and Hay, J. L., 2001, "On the Measurement of Stress-Strain Curves by Spherical Indentation," Thin Solid Films, 398-399, pp. 331-335.

Hill, R., Storåkers, B., and Zdunek, A. B., 1989, "A Theoretical Study of the Brinell Hardness Test," Proceedings of the Royal Society (London), Series A, 436, pp. 301-330.

Huber, N., Konstantinidis, A., and Tsakmakis, Ch., 2001, "Determination of Poisson's Ratio by Spherical Indentation Using Neural Networks – Part I: Theory," ASME Journal of Applied Mechanics, 68, pp. 218-223.

Johnson, K. L., 1970, "The Correlation of Indentation Experiments," Journal of the Mechanics and Physics of Solids, 18, pp. 115-126.

Johnson, K. L., 1985, Contact Mechanics, Cambridge University Press, Cambridge, UK, pp. 90-95 and 170-184.

Komvopoulos, K., and Yan, W., 1998, "Three-Dimensional Elastic-Plastic Fractal Analysis of Surface Adhesion in Microelectromechanical Systems," ASME Journal of Tribology, 120, pp. 808-813.

Komvopoulos, K., and Ye, N., 2001, "Three-Dimensional Contact Analysis of Elastic-Plastic Layered Media With Fractal Surface Topographies," ASME Journal of Tribology, 123, pp. 632-640.

Kral, E. R., Komvopoulos, K., and Bogy, D. B., 1993, "Elastic-Plastic Finite Element Analysis of Repeated Indentation of a Half-Space by a Rigid Sphere," ASME Journal of Applied Mechanics, 60, pp. 829-841.

Kucharski, S., and Mroz, Z., 2001, "Identification of Plastic Hardening Parameters of Metals from Spherical Indentation Tests," Materials Science and Engineering A, 318, pp. 65-76.

Liu, G., Wang, Q. J., and Lin, C., 1999, "A Survey of Current Models for Simulating the Contact Between Rough Surfaces," Tribology Transactions, 42, pp 581-591.

Marsh, D. M., 1964, "Plastic Flow in Glass," Proceedings of the Royal Society (London), Series A, 279, pp. 420-435.

Mesarovic, S. Dj., and Fleck, N. A., 1999, "Spherical Indentation of Elastic-Plastic Solids," Proceedings of the Royal Society (London), Series A, 455, pp. 2707-2728.

Nayebi, A., El Abdi, R., Bartier, O., and Mauvoisin, G., 2002, "New Procedure to Determine Steel Mechanical Parameters from the Spherical Indentation Technique," Mechanics of Materials, 34, pp. 243-254.

Oliver, W. C., and Pharr, G. M., 1992, "An Improved Technique for Determining Hardness and Elastic Modulus Using Load and Displacement Sensing Indentation Experiments," Journal of Materials Research, 7, pp. 1564-1583.

Sahoo, P., and Roy Chowdhury, S. K., 2000, "A Fractal Analysis of Adhesive Friction Between Rough Solids in Gentle Sliding," Proc. Instn. Mech. Engrs., Part J, 214, pp. 583-595.

Sneddon, I. N., 1965, "The relation Between Load and Penetration in the Axisymmetric Boussinesq Problem for a Punch of Arbitrary Profile," International Journal of Engineering Science, 3, pp. 47-57.

Tabor, D., 1951, The Hardness of Metals, Clarendon Press, Oxford, UK.

Thurn, J., Morris, D. J., and Cook, R. F., 2002, "Depth-Sensing Indentation at Macroscopic Dimensions," Journal of Materials Research, 17, pp. 2679-2690.

Vu-Quoc, L., Zhang, X., and Lesburg, L., 2000, "A Normal Force-Displacement Model for Contacting Spheres Accounting for Plastic Deformation: Force-Driven Formulation," ASME Journal of Applied Mechanics, 67, pp. 363-371.

Ye, N., and Komvopoulos, K., 2003, "Indentation Analysis of Elastic-Plastic Homogeneous and Layered Media: Criteria for Determining the Real Material Hardness," ASME Journal of Tribology, 125, (in press).

List of Figures

Fig. 1. Schematic of spherical indentation and pertinent nomenclature.

Fig. 2. Finite element model for indentation analysis. (The inset at the top shows the finesse of the mesh near the surface.).

Fig. 3. Comparison of analytical (Hertz) and finite element results for the dimensionless mean contact pressure, p_m/Y, versus dimensionless interference, d/r', in the elastic deformation regime for $E/Y = 11$.

Fig. 4. Dimensionless mean contact pressure, p_m/Y, versus dimensionless interference, d/r', in the elastic-plastic and fully plastic deformation regimes for different material properties, E/Y.

Fig. 5. Dimensionless hardness, H/Y, versus material properties, E/Y.

Fig. 6. Deformation map of dimensionless interference, d/r', versus material properties, E/Y, showing the boundaries between elastic, elastic-plastic, and fully plastic deformation regimes.

Fig. 7. Dimensionless contact area, a'/a, versus dimensionless interference, d/r', in the elastic-plastic deformation regime.

Fig. 8. Elastic and plastic regions in the half-space due to indentation loading at the inception of fully plastic deformation and full unloading: (a) $E/Y = 11$ and (b) $E/Y = 450$.

Fig. 9. Normalized strain versus material properties, E/Y, at the inception of fully plastic deformation.

Fig. 10. Radial distance of material point where the maximum equivalent plastic strain occurs at the inception of fully plastic deformation, x/r, versus material properties, E/Y.

Fig. 11. Elastic recovery, E_R, upon unloading from the inception of fully plastic deformation determined from the displacement at the center of the residual impression (Eq. (12)) and the elastic strain energy release (Eq. (13)) versus material properties, E/Y.

Fig. 12. Error in contact area at the inception of fully plastic deformation, e_a, versus material properties, E/Y. (The error is calculated as the difference between the area of the residual impression, a_i, or the area determined from the shape function of the spherical indenter, a_s, and the real contact area at the inception of unloading, a.).

Fig. 13. Error in reduced elastic modulus at the inception of fully plastic deformation, e_E, versus material properties, E/Y. (The error is calculated as the difference between the elastic modulus determined from Eq. (5) using the contact area at the inception of unloading, a, the residual impression area, a_i, or the area determined from the shape function of the spherical indenter, a_s, and the real elastic modulus used in the finite element simulations.).

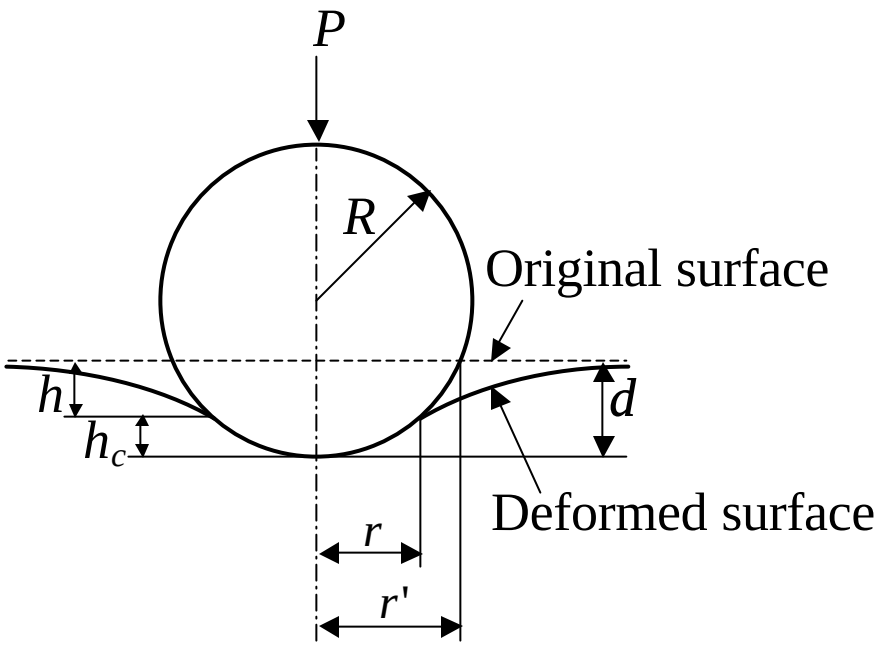

Fig. 1. Schematic of spherical indentation and pertinent nomenclature.

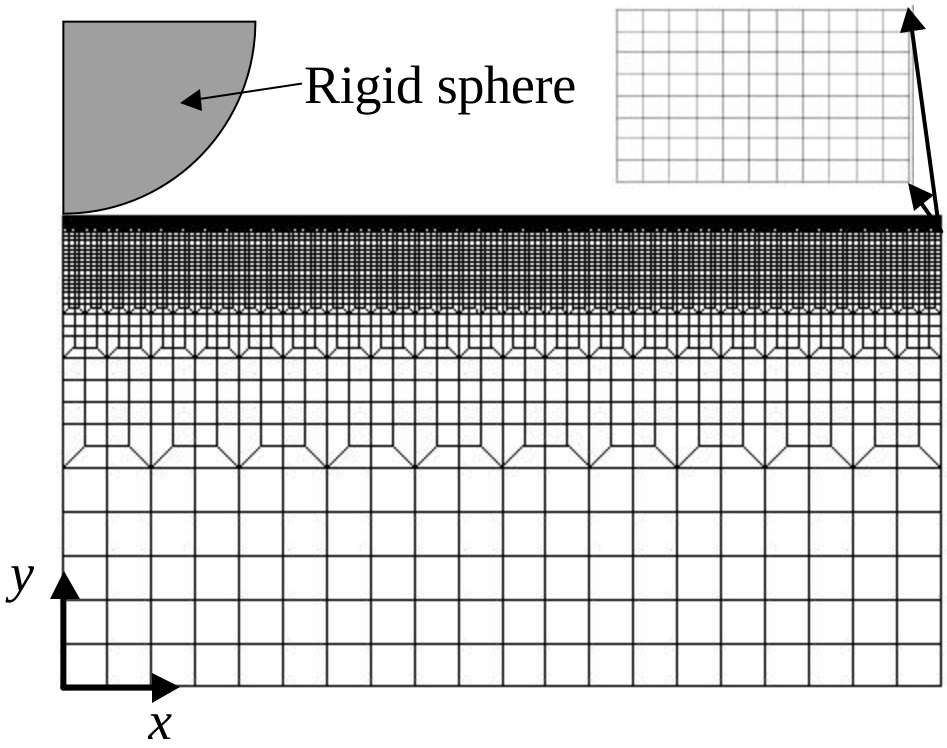

Fig. 2. Finite element model for indentation analysis. (The inset at the top shows the finesse of the mesh near the surface.).

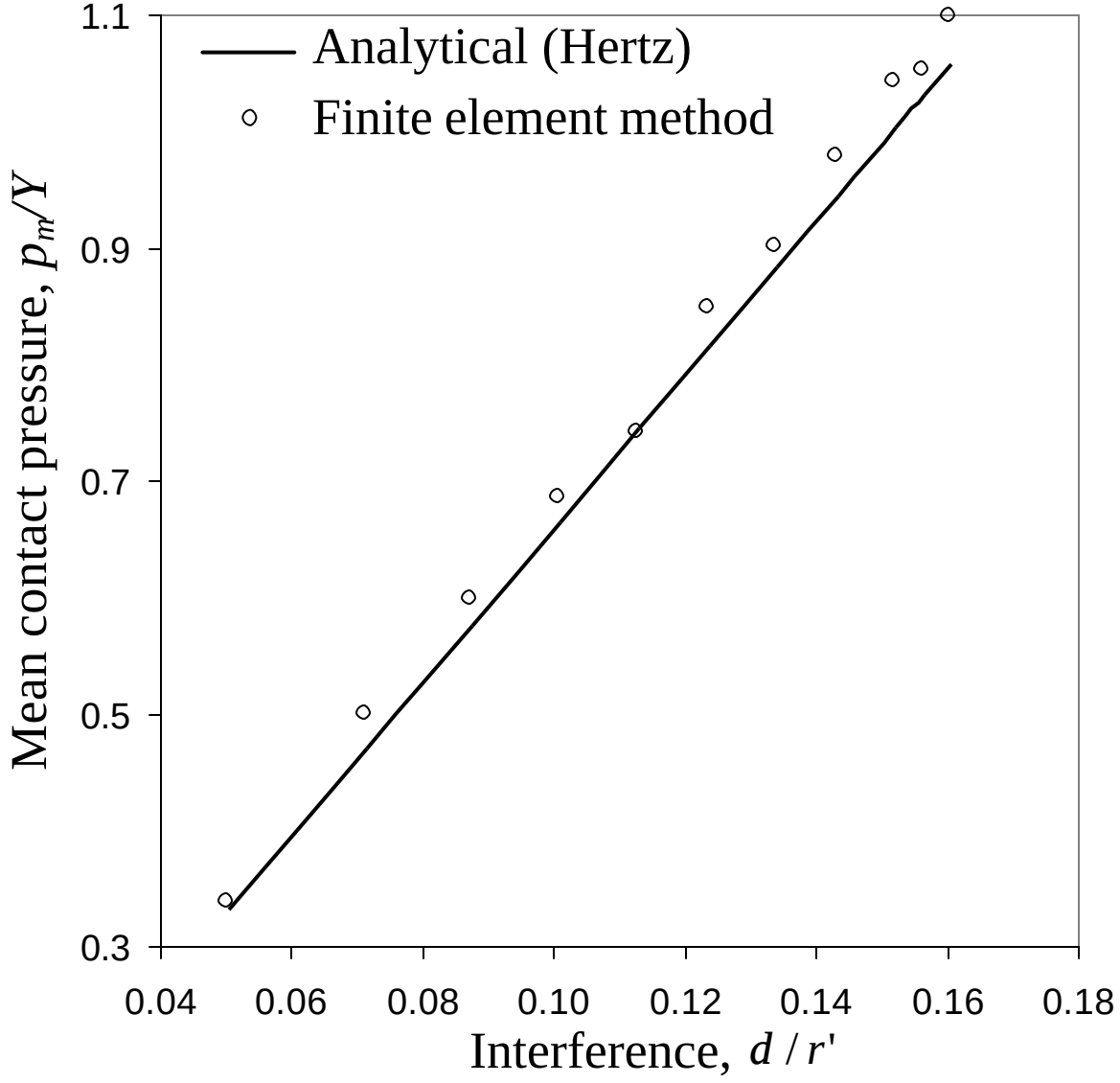

Fig. 3. Comparison of analytical (Hertz) and finite element results for the dimensionless mean contact pressure, p_m/Y, versus dimensionless interference, d / r', in the elastic deformation regime for $E/Y = 11$.

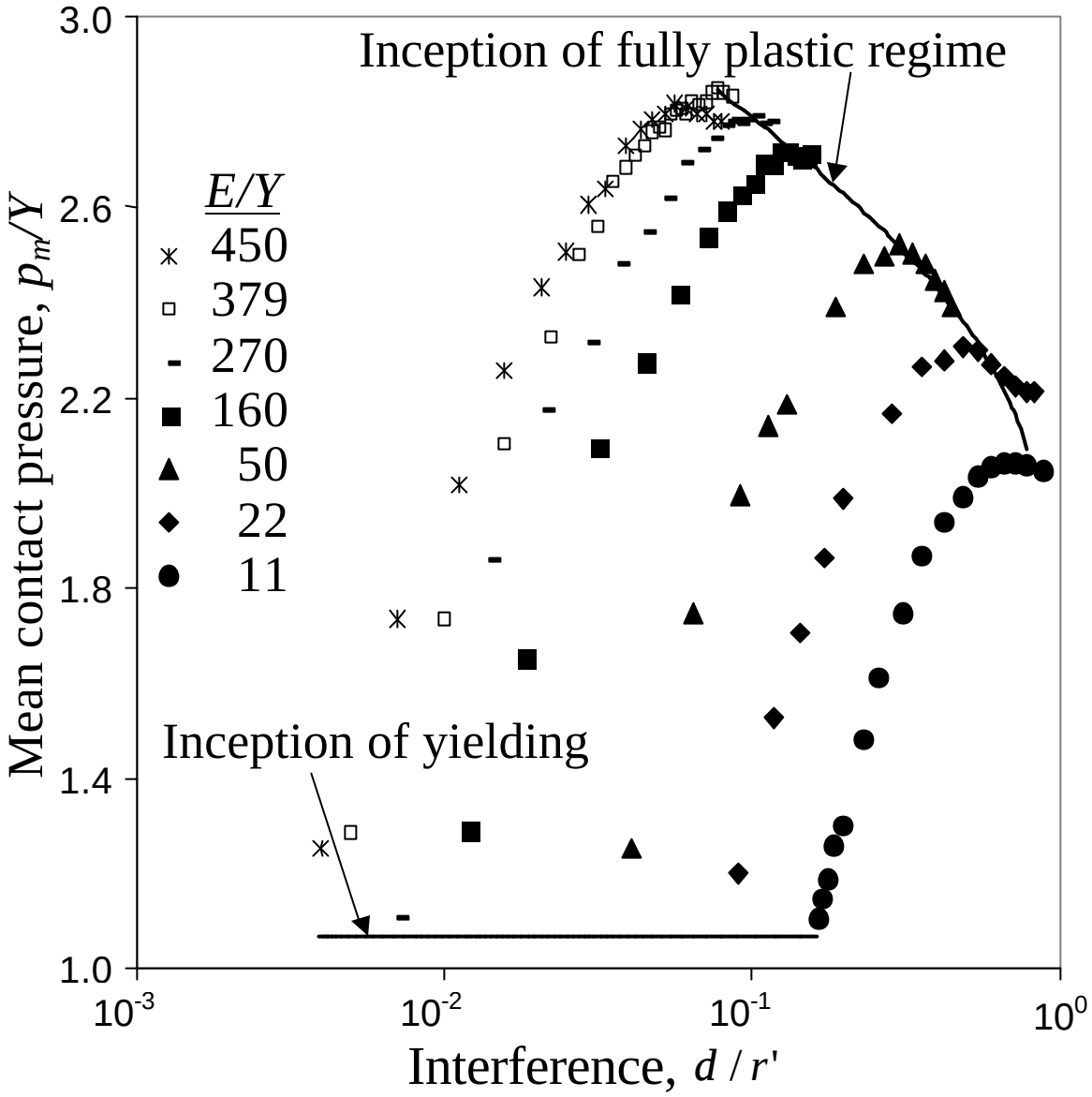

Fig. 4. Dimensionless mean contact pressure, p_m/Y, versus dimensionless interference, d / r', in the elastic-plastic and fully plastic deformation regimes for different material properties, E/Y.

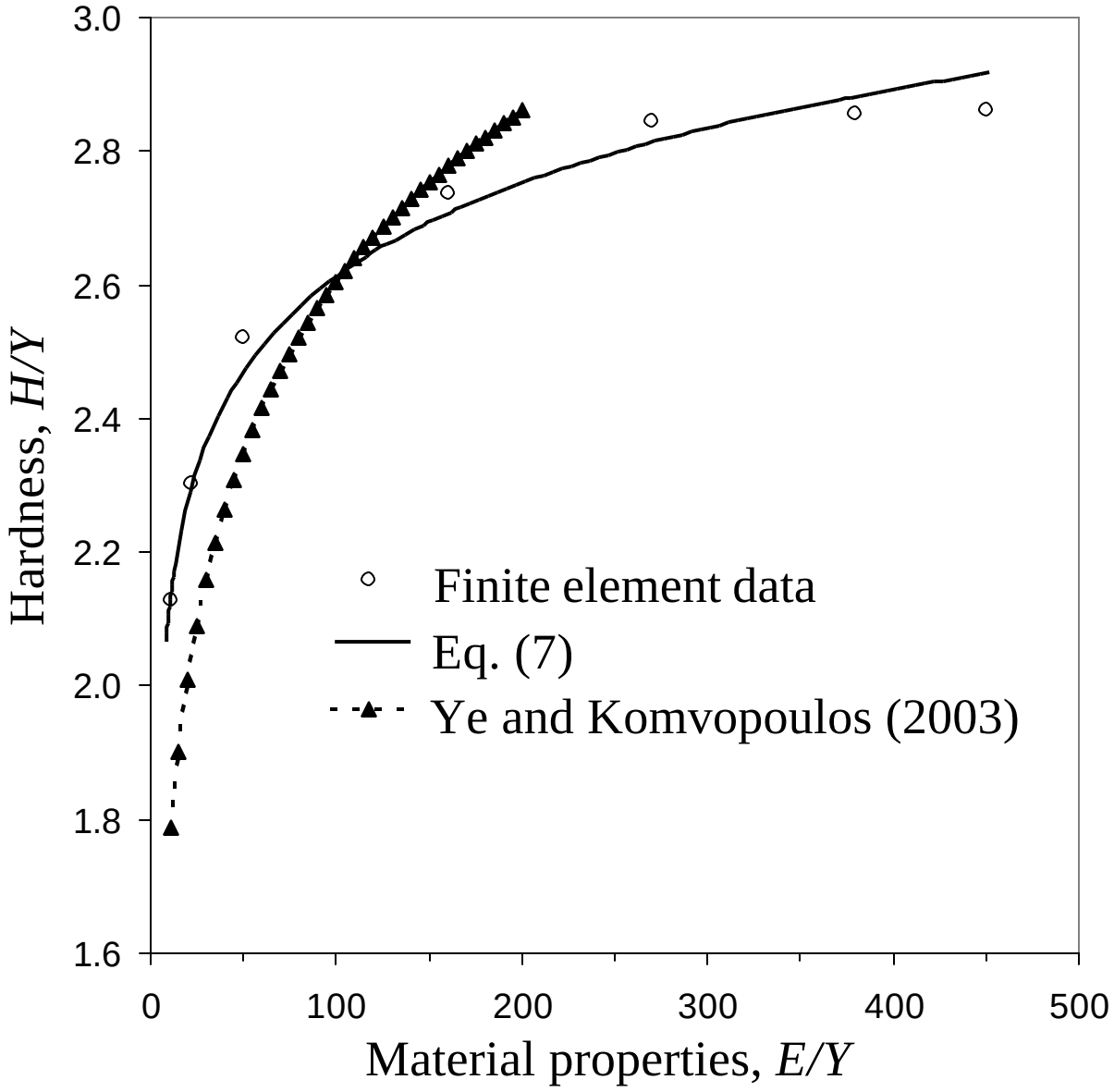

Fig. 5. Dimensionless hardness, *H/Y*, versus material properties, *E/Y*.

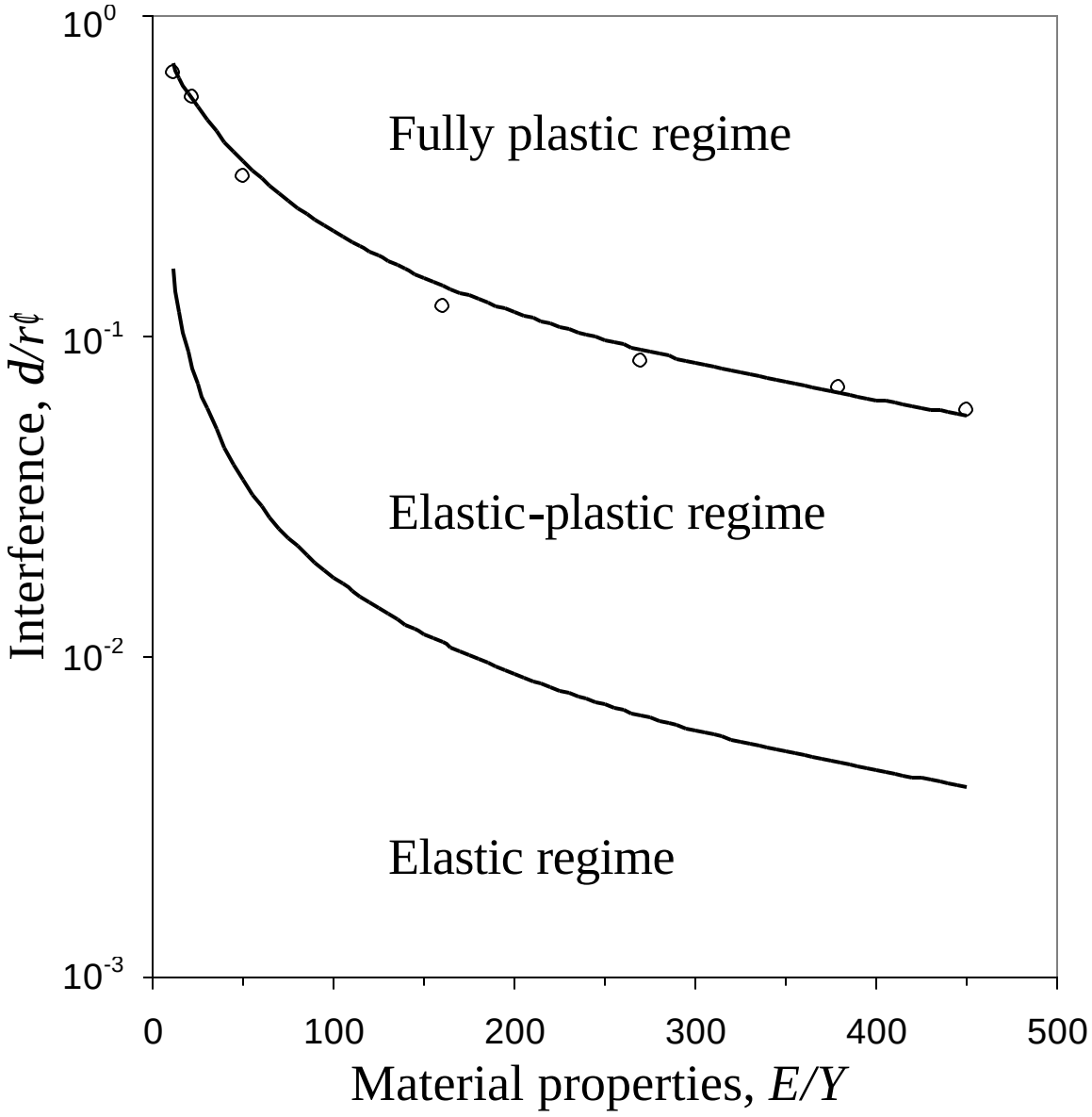

Fig. 6. Deformation map of dimensionless interference, d/r', versus material properties, E/Y, showing the boundaries between elastic, elastic-plastic, and fully plastic deformation regimes.

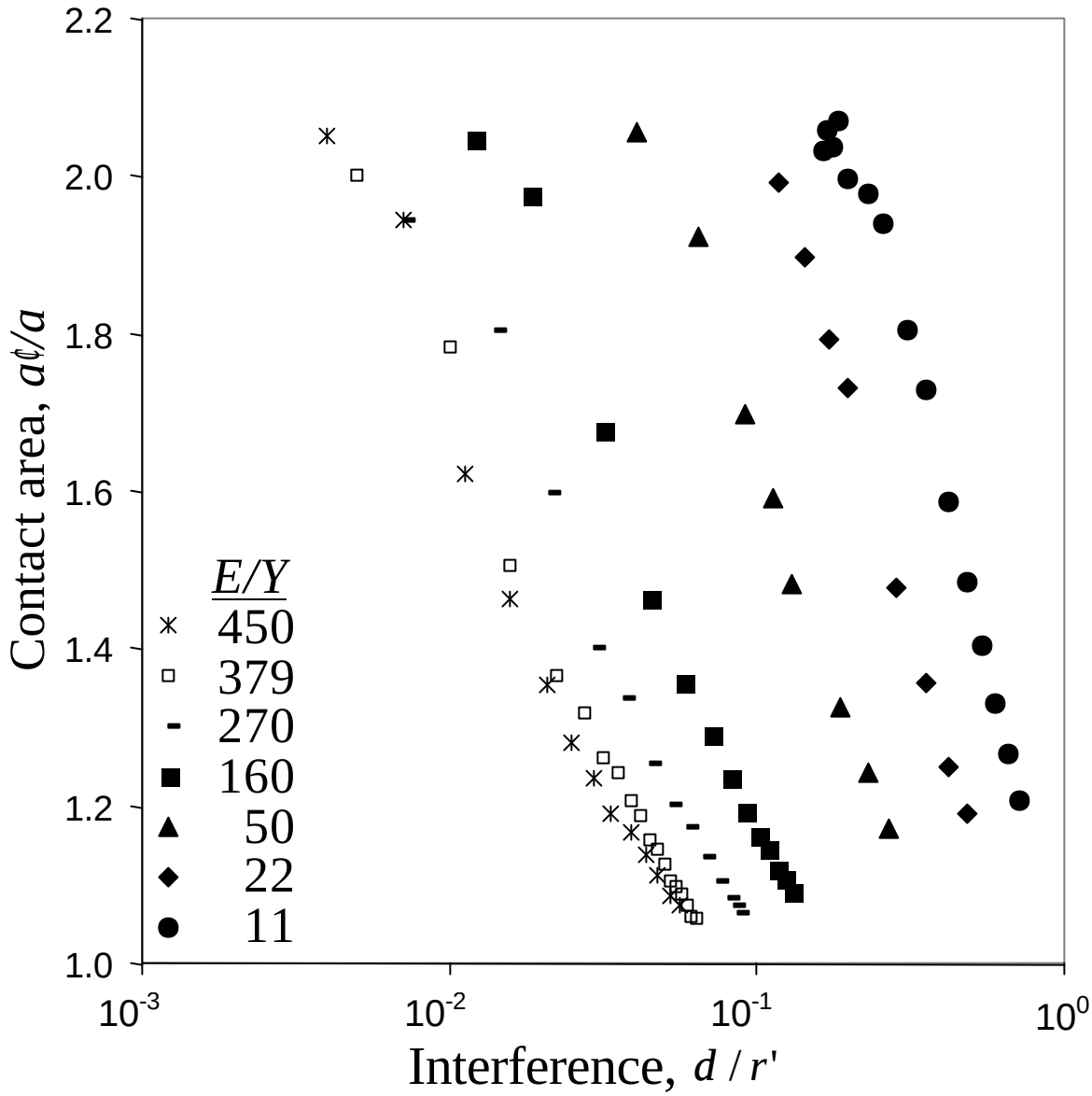

Fig. 7. Dimensionless contact area, a'/a, versus dimensionless interference, d/r', in the elastic-plastic deformation regime.

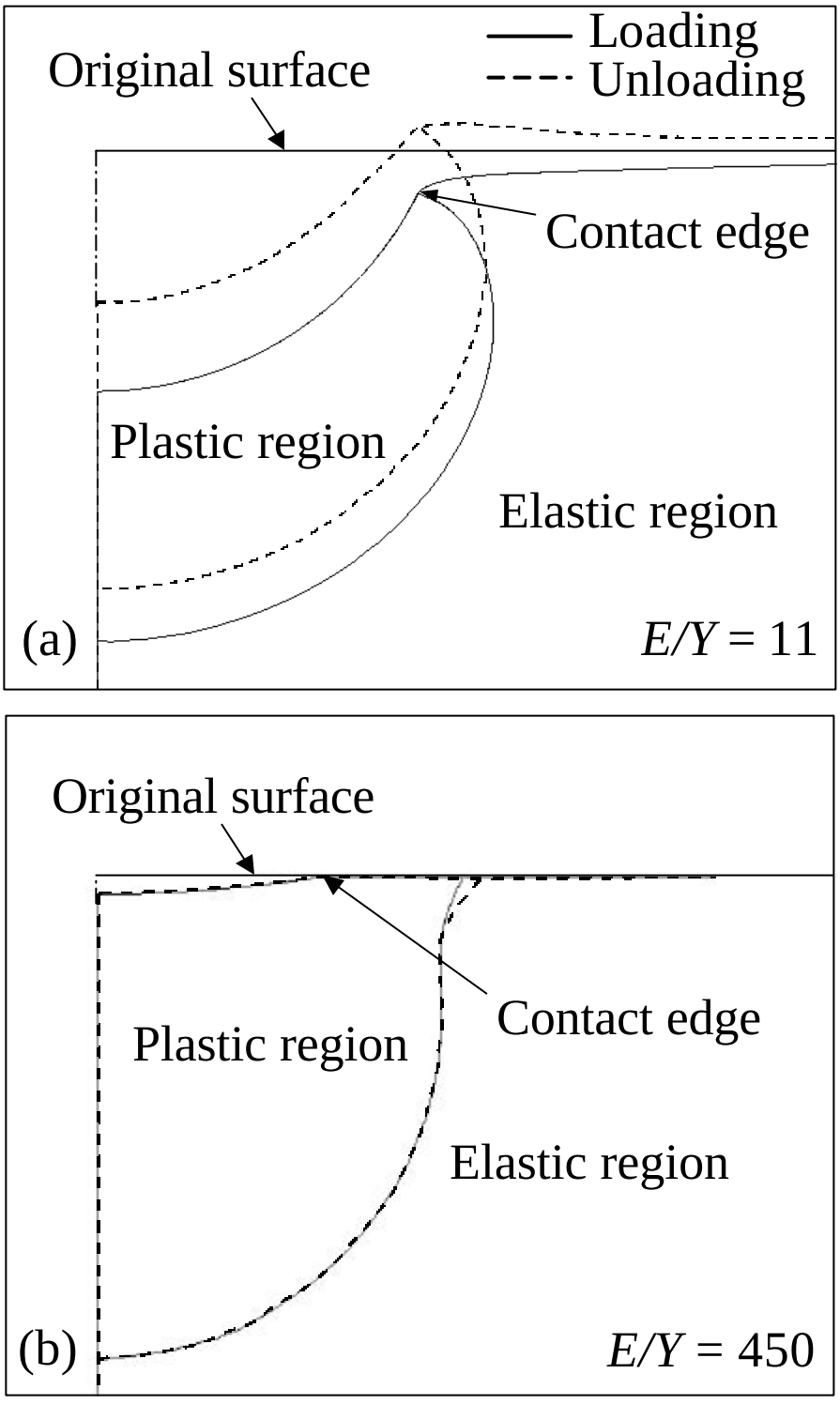

Fig. 8. Elastic and plastic regions in the half-space due to indentation loading at the inception of fully plastic deformation and full unloading: (a) $E/Y = 11$ and (b) $E/Y = 450$.

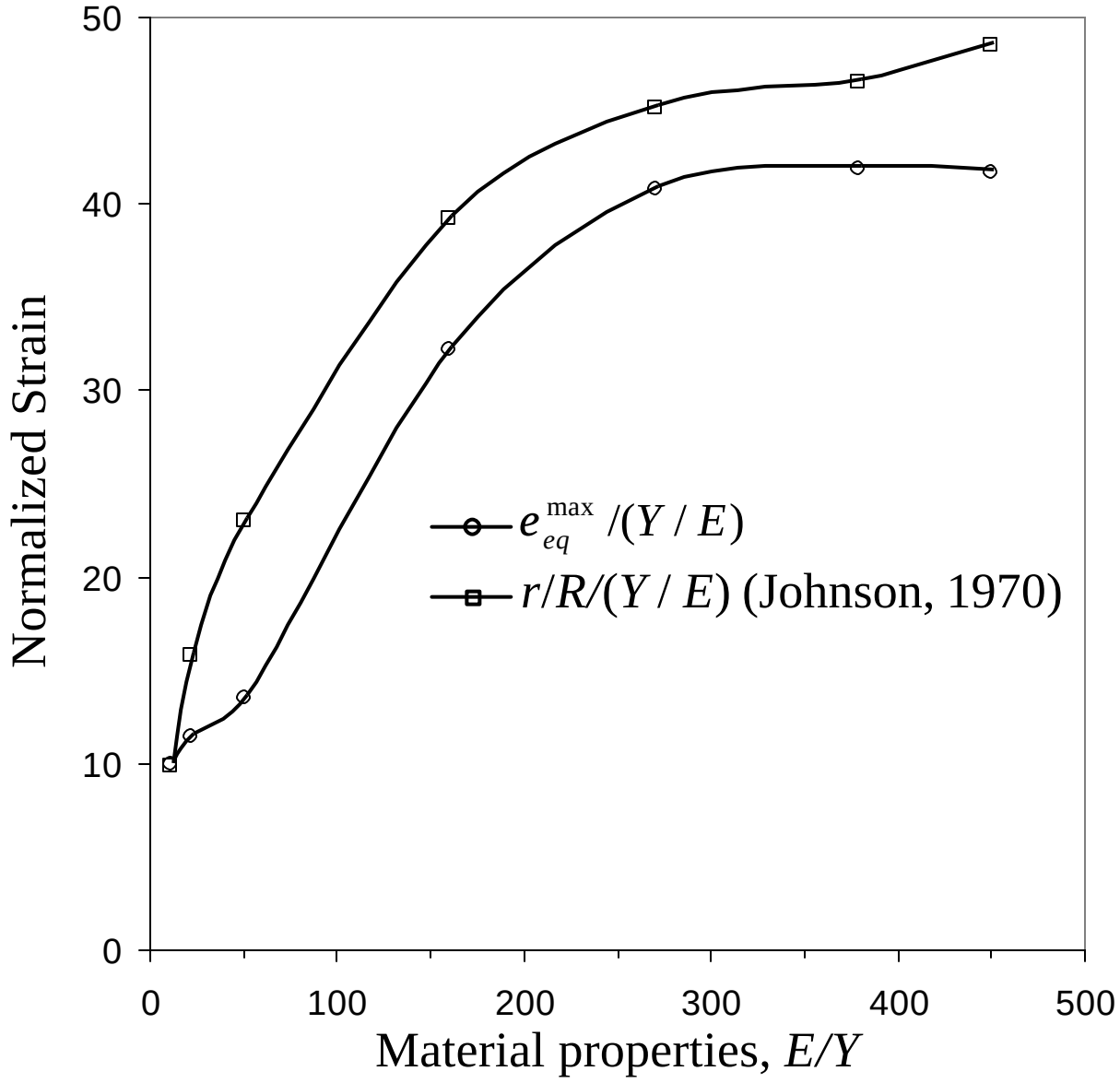

Fig. 9. Normalized strain versus material properties, *E/Y*, at the inception of fully plastic deformation.

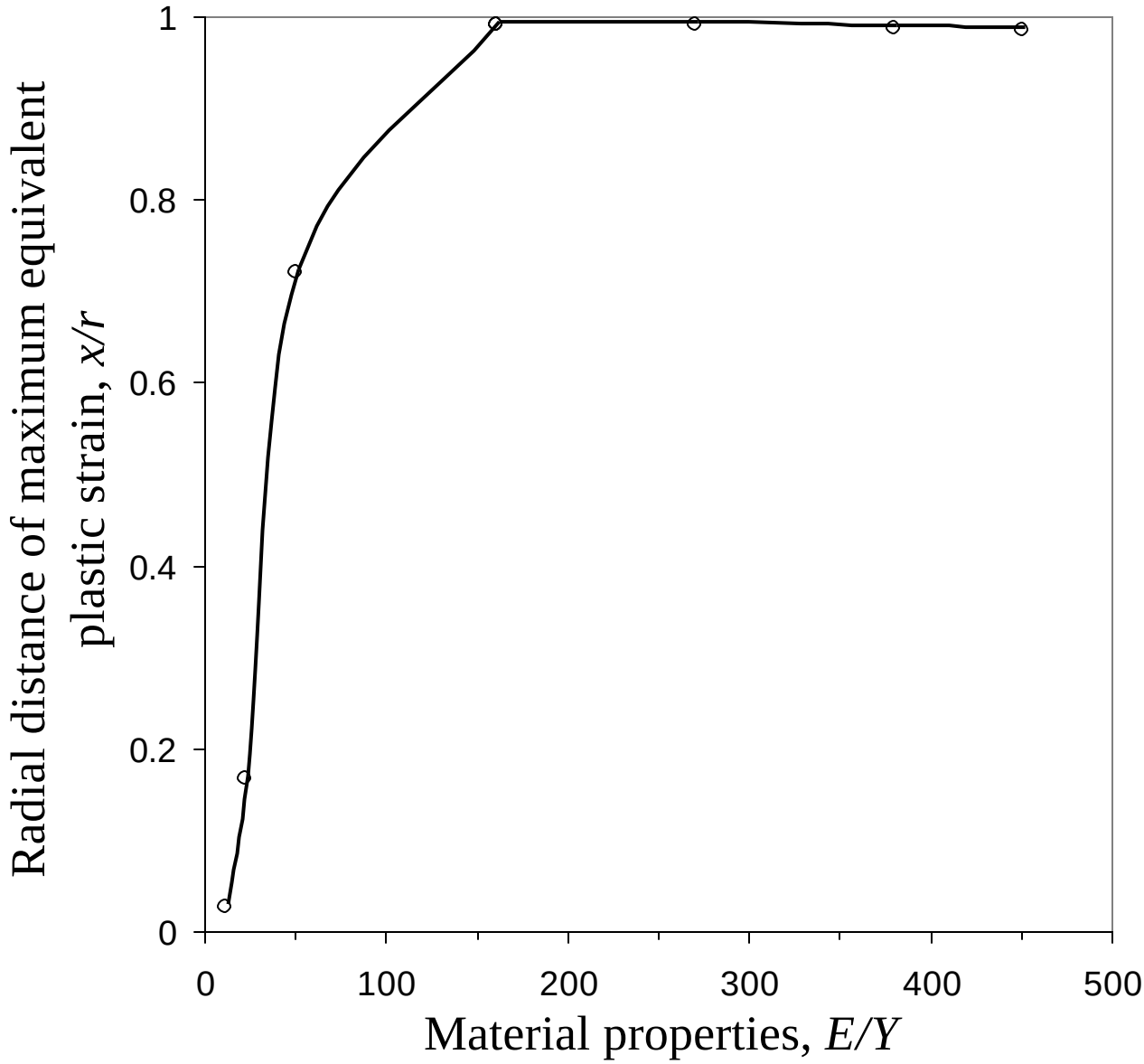

Fig. 10. Radial distance of material point where the maximum equivalent plastic strain occurs at the inception of fully plastic deformation, *x/r*, versus material properties, *E/Y*.

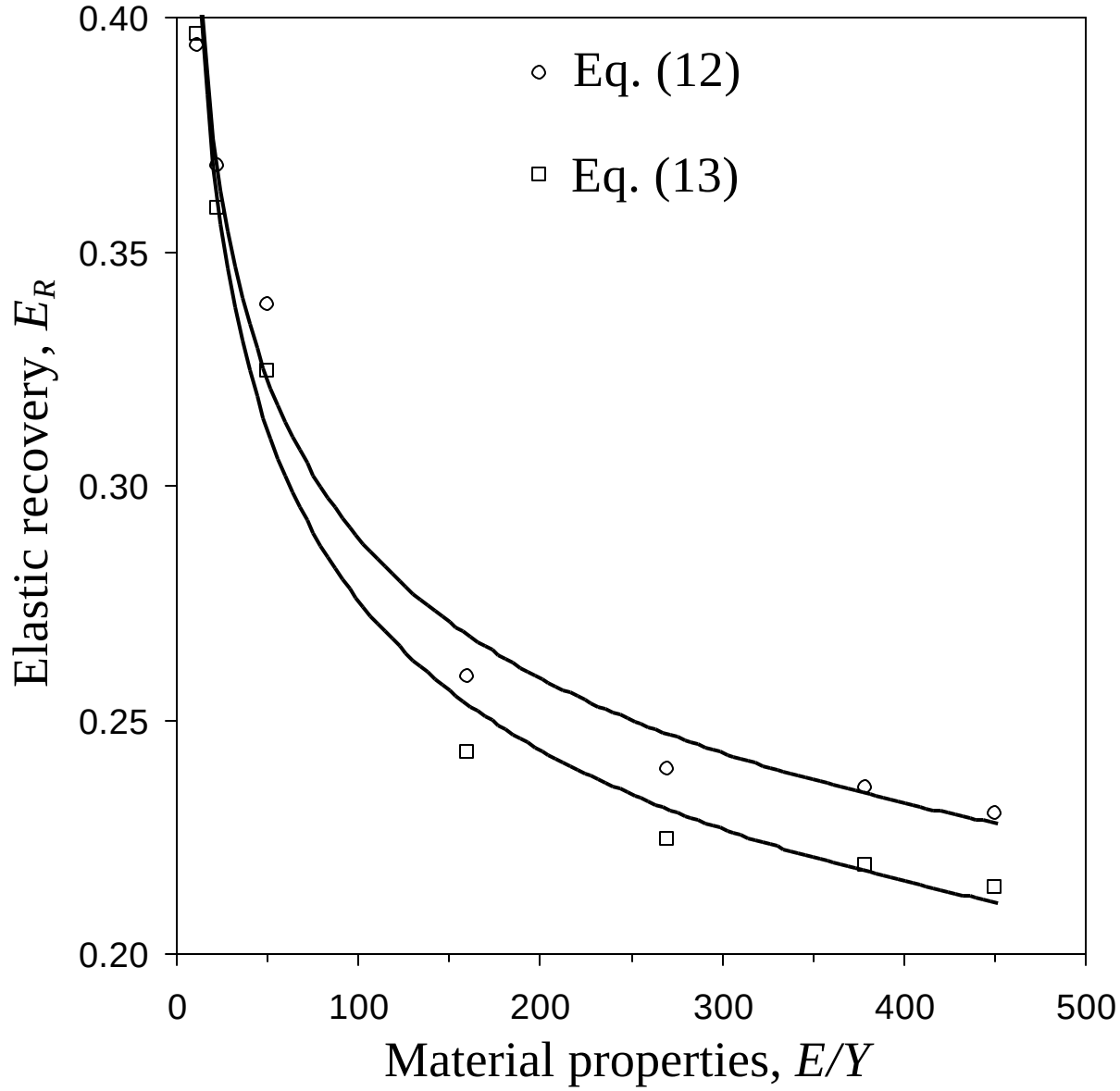

Fig. 11. Elastic recovery, E_R, upon unloading from the inception of fully plastic deformation determined from the displacement at the center of the residual impression (Eq. (12)) and the elastic strain energy release (Eq. (13)) versus material properties, E/Y.

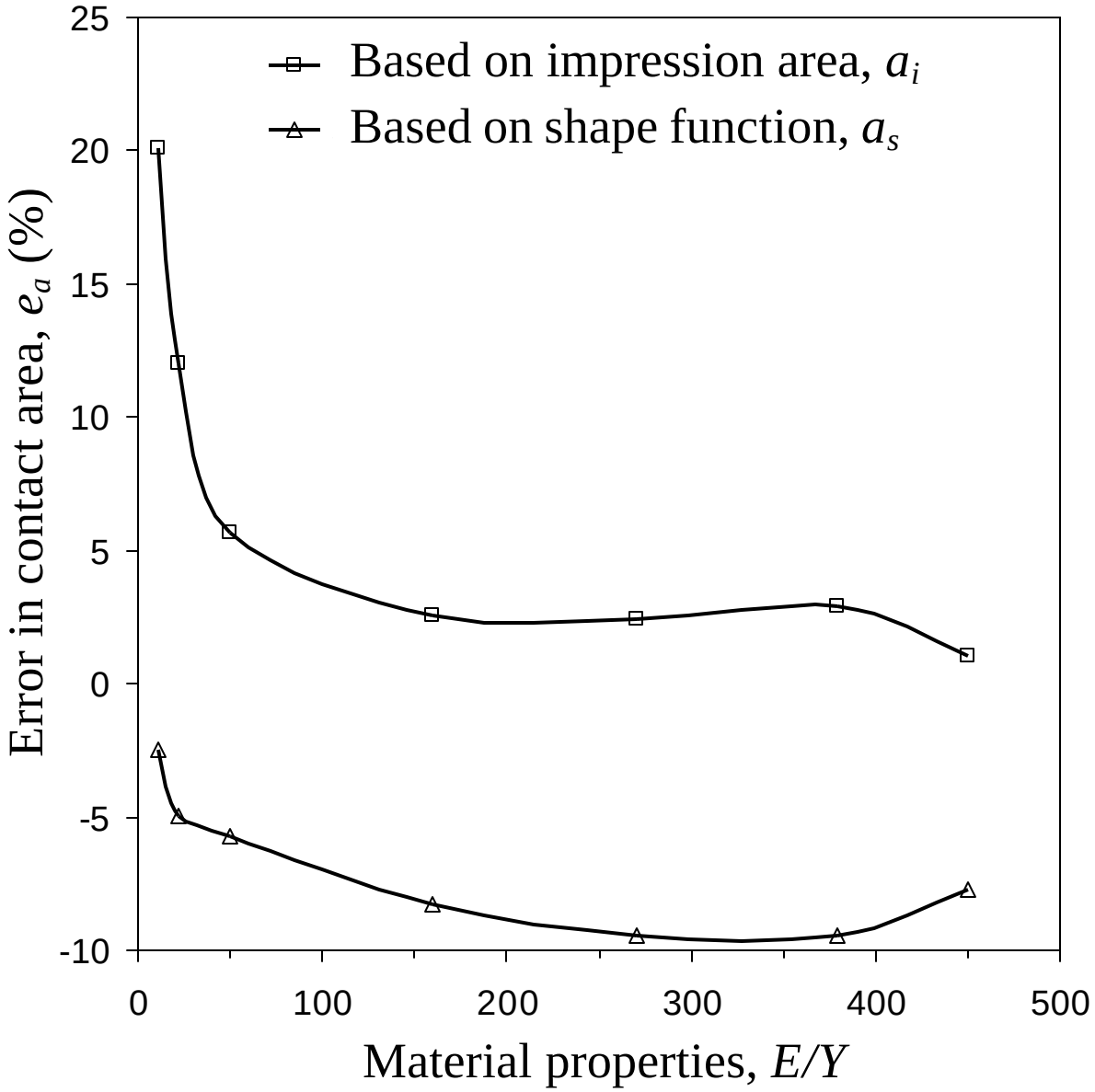

Fig. 12. Error in contact area at the inception of fully plastic deformation, e_a, versus material properties, E/Y. (The error is calculated as the difference between the area of the residual impression, a_i, or the area determined from the shape function of the spherical indenter, a_s, and the real contact area at the inception of unloading, a.).

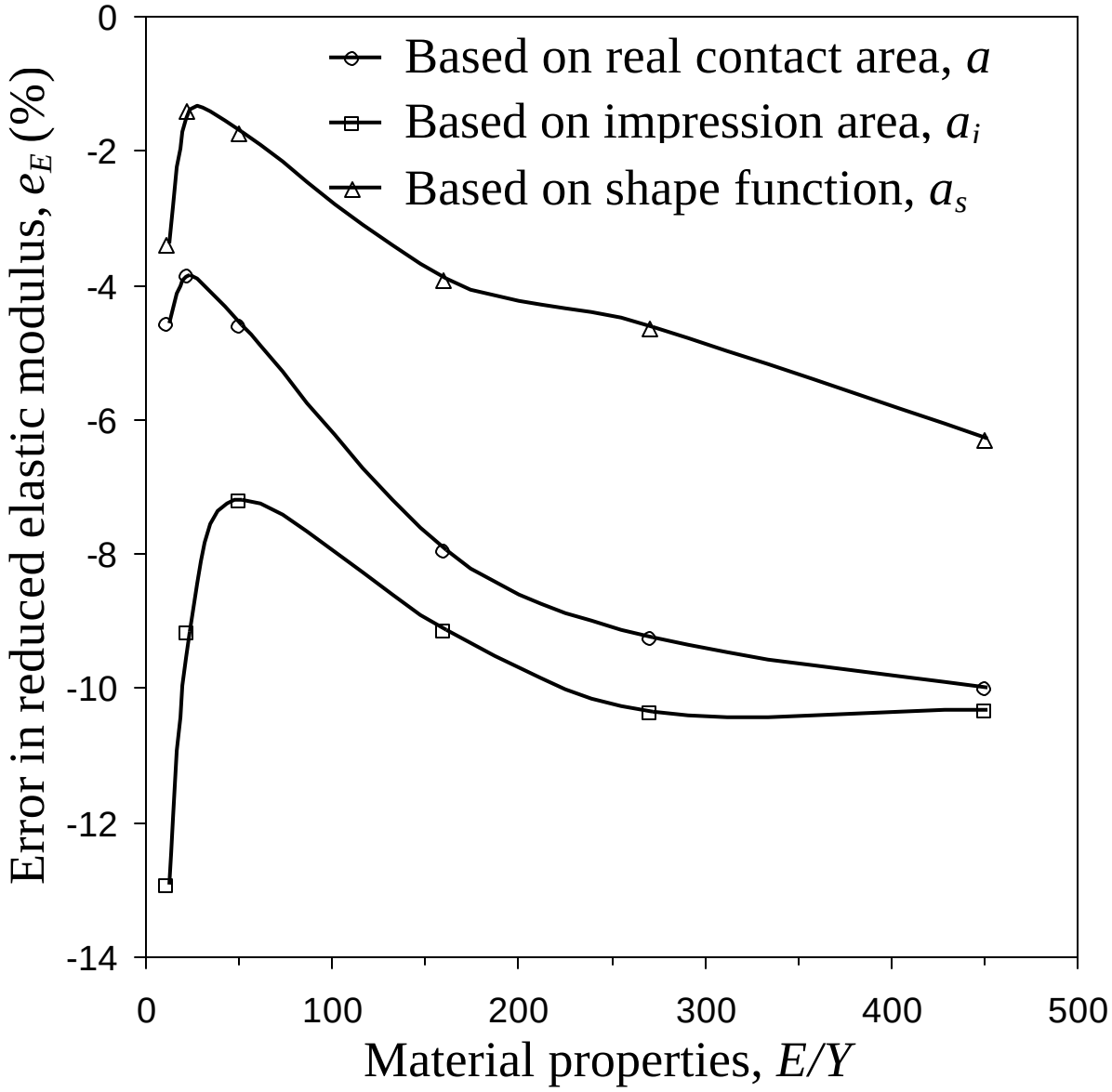

Fig. 13. Error in reduced elastic modulus at the inception of fully plastic deformation, e_E, versus material properties, E/Y. (The error is calculated as the difference between the elastic modulus determined from Eq. (5) using the contact area at the inception of unloading, a, the residual impression area, a_i, or the area determined from the shape function of the spherical indenter, a_s, and the real elastic modulus used in the finite element simulations.).